Applied Catalysis B: Environmental 123–124 (2012) 296–305

Contents lists available at SciVerse ScienceDirect

Applied Catalysis B: Environmental

journal homepage: www.elsevier.com/locate/apcatb

Effect of C_3H_6 on selective catalytic reduction of NO_x by NH_3 over a Cu/zeolite catalyst: A mechanistic study

Jin-Yong Luo[a], Harry Oh[a], Cary Henry[b], William Epling[a,*]

[a] Department of Chemical Engineering, University of Waterloo, 200 University Ave W, Waterloo, ON, N2L 3G1, Canada
[b] Cummins Inc, 1900 McKinley Ave., Columbus, IN 47201, United States

ARTICLE INFO

Article history:
Received 16 February 2012
Received in revised form 20 April 2012
Accepted 23 April 2012
Available online 28 April 2012

Keywords:
Selective catalytic reduction
NO_x control
Diesel emissions
Transient-response method
In situ DRIFTS
Catalyst poisoning

ABSTRACT

The effects of C_3H_6 on key SCR reactions over a model Cu/beta zeolite catalyst were characterized using step-response method reactor testing. Under standard SCR conditions, C_3H_6 clearly inhibited the reduction reaction at 200 °C and above. The inhibition was not caused by competitive adsorption between C_3H_6 and NH_3, but by surface intermediate species formed during C_3H_6 oxidation, including acrolein-like and coke species as indicated by in situ DRIFTS. Similar to the standard SCR reaction, C_3H_6 also had a negative effect on the fast SCR reaction. Spaci-FTIR (spatially resolved capillary-inlet Fourier transform infrared spectroscopy) results indicated that NO_2 was quickly reduced to NO by C_3H_6, leading to the occurrence of some standard SCR instead of purely fast SCR. However, C_3H_6 had a positive effect on NO_2 SCR. The reduction of NO_2 to NO by C_3H_6 resulted in the occurrence of the fast SCR reaction combined with NO_2 SCR instead of pure NO_2 SCR. The reaction pathway change also decreased N_2O formation significantly.

1. Introduction

Selective catalytic reduction of NO_x by NH_3 (NH_3-SCR) has become a leading NO_x emission control technology for diesel and lean-burn gasoline engine exhaust, due to advancements in catalyst development and system improvements [1]. NH_3, as the reductant, can be supplied either by urea hydrolysis, or formed on upstream lean NO_x traps (LNTs), three way catalysts (TWCs), or hydrocarbon-SCR catalysts [2–5]. The corresponding catalysts mainly consist of iron or copper supported on zeolites. The zeolite materials also serve as a reservoir for NH_3, critical for passive SCR applications, where the NH_3 is generated during a reductant-rich phase on upstream TWC or LNT catalysts. In general, under standard SCR conditions, Fe/zeolite performs well for high temperature applications while Cu/zeolite shows excellent activity at low temperatures. The intrinsic reason is that the SCR activity over Fe/zeolite is self-inhibited by NH_3 due to its strong adsorption on iron sites at low temperature, whereas it is minimally affected by NH_3 adsorption over a Cu/zeolite [6].

Two types of deactivation that are commonly seen in automotive catalysts also apply to SCR catalysts: thermal aging and chemical fouling [7–12]. Thermal aging can lead to sintering of the active metal sites and irreversible zeolite structure collapse via dealumination. High temperatures on the SCR catalyst can be reached, for example, during particulate filter regeneration. Significant progress has been made in terms of improving the thermal stability of SCR catalysts. For example, recent studies indicate that SCR catalysts made of copper on zeolites with a small pore structure, such as zeolite SSZ-13 and SAPO-34 with a chabazite structure, are durable against high temperature exposure and lean-rich aging [8,13,14]. Chemical aging involves the poisoning or blocking of the active sites, by species such as hydrocarbons (HCs), soot, potassium, etc. [10–12]. Some of the poisons can be removed by simply exposing the catalyst to high temperatures.

The focus of the study performed is hydrocarbon poisoning. During cold start, or if the upstream DOC catalyst is deactivated via thermal aging, hydrocarbons may slip through the DOC and interact with downstream NH_3-SCR catalysts. Although hydrocarbons can be considered as a reductant in a HC-SCR process, they are considered poisons for NH_3-SCR catalysts [15–23]. In the literature, several mechanisms have been proposed for HC poisoning, including competitive adsorption between the HCs and NH_3, coke formation which blocks pores and/or active sites, inhibition of the formation of required intermediates such as NO_2, and thermal aging caused by residual hydrocarbon burning. For example, Heo et al. proposed that over Cu/ZSM5 and Fe/ZSM5 catalysts, the primary cause for C_3H_6 inhibition on NH_3-SCR was the competitive adsorption of NH_3 and C_3H_6 on the catalyst surface [15]. On the other hand, Li et al. found that NH_3 adsorption was not hindered on a C_3H_6-poisoned Fe-ZSM5 catalyst, and proposed that the deactivation

* Corresponding author.
E-mail address: wsepling@uh.edu (W. Epling).

0926-3373/$ – see front matter
http://dx.doi.org/10.1016/j.apcatb.2012.04.038

mechanism was iron active sites being blocked by carbonaceous deposits, which limits NO oxidation to NO_2, a crucial step in the overall SCR reaction [16]. Furthermore, over Fe-zeolite catalysts, it has been shown that SCR performance is a function of HC speciation and reaction temperature. Using DRIFTS, Malpartida et al. investigated the effect of multiple HC species, including C_3H_6, C_7H_8 and $C_{10}H_{22}$, on NH_3-SCR over a Fe-zeolite catalyst, and concluded that HCs compete with NH_3 for adsorption sites and lower NO_x conversion. The competition was strongest with $C_{10}H_{22}$ and negligible with C_3H_6 [18]. Devarakonda et al. found that the poisoning effect of C_7H_8 on NH_3-SCR over a Fe-zeolite was caused by blocking active sites where NH_3 adsorbs, with the extent depending on temperature. Toluene has a significantly negative effect at low temperature due to strong adsorption, but the impact decreases at higher temperatures [19].

Similarly, for Cu-based catalysts, the SCR performance is also a function of hydrocarbon species, temperature, as well as zeolite type. Researchers from Ford found that for an early generation Cu-based catalyst, the NO_x activity inhibition decreases in the order of $C_{10}H_{22} \gg C_6H_6 \approx C_2H_4$. While for a state-of-the-art Cu-zeolite catalyst, long chain hydrocarbons like $C_{10}H_{22}$ and C_6H_6 have no effect on the activity, while C_3H_6 still has some negative effect [20]. Sultana et al. also pointed out that small pore zeolite catalysts, such as Cu-FER, show higher poisoning resistance to $C_{10}H_{22}$, as compared to copper zeolites with relatively larger pores, such as ZSM-5 and MOR, because of less HC deposition [21,22]. Regardless of the zeolite type, C_3H_6 still has a negative effect due to its smaller molecule size.

With respect to the effect of C_3H_6 on copper-based zeolites, it is interesting to note that there is a negative effect observed primarily in the medium temperature range (~300 °C), while at both low and high temperatures, the effect on NO_x conversion is small or negligible [11,15]. Multiple mechanisms have been proposed. Heo proposed that on the Cu/ZSM5 surface, competitive adsorption between C_3H_6 and NH_3 occurs at low temperature, and the interaction, or ammoxidation, between them consumes reductant NH_3 at medium temperature [11]. On the other hand, Cavataio found that less NH_3 was consumed in the presence of C_3H_6, and proposed that coke deposits generated during C_3H_6 exposure deactivated the catalyst, since the activity after long-term C_3H_6 exposure (2 h) decreased to a larger extent when compared with the activity after short-term exposure (30 s). On this basis, there is still some debate concerning the deactivation mechanism. In order to better understand this process, a step-response method was employed in this study to explore both the transient and long-term poisoning mechanisms of C_3H_6 on NH_3-SCR. In situ DRIFTS was used to identify types of poisons, and spaci-FTIR was used to resolve both the transient and long-term behavior. The effect of C_3H_6 on fast-SCR (where an equimolar amounts of NO and NO_2 are added) and NO_2-SCR (pure NO_2 as the NO_x feed) was also investigated.

2. Experimental methods

The catalyst used in this study was a model Cu/beta zeolite supplied by Cummins. The beta zeolite sample had a SiO_2/Al_2O_3 ratio of 25. The Cu loading was 3.5% by weight of the zeolite, with a total loading of 130 g/L. A core, 1.0″ (diameter) × 1.5″ (length), wrapped with 3 M matting materials to prevent gas bypass, was inserted into a quartz tube reactor that was mounted in a Lindberg Minimite furnace for sample heating. Small hollow quartz tubes were placed in the reactor, positioned upstream of the catalyst in order to improve gas distribution and preheating. Two thermocouples were inserted into the catalyst monolith in order to record inlet and outlet core temperatures. The temperatures shown in all figures were obtained by averaging these two temperatures, while a maximum difference of 10 °C was noted at the highest temperature tested. Before the testing, the catalyst was degreened at 550 °C for 4 h in an oxidizing environment (8% O_2, 5% CO_2 and 2.5% H_2O, balance N_2).

The gases and gas mixtures, except balance N_2, were supplied by Praxair and were metered with Bronkhorst mass flow controllers. Balance N_2 was produced by a N_2 generator manufactured by On-Site. Water was introduced by a Bronkhorst CEM system. All the gas lines were heated and maintained at ~120 °C to prevent water from condensing in the lines. In this study, a step-response method was employed in order to evaluate both the transient and long-term response to gas concentration changes. NH_3 and C_3H_6 were introduced directly in front of the reactor via a three-way switching valve, thus being directed either into the reactor or to vent. The feed gas composition, when all gases were added, was 600 ppm NH_3, 600 ppm NO_x, 200 ppm C_3H_6, 8% O_2, 5% CO_2 and 2.5% H_2O, at a space velocity of 28,000 h^{-1} (STP). A MKS MultiGas 2030 FTIR analyzer was used for gas concentration measurements.

Spatially resolved gas concentration data were obtained by slightly modifying the inlet to the MultiGas 2030 system. A small amount of gas, which was sampled by a fused silica capillary (ID = 0.32 mm, OD = 0.43 mm, L = 30 cm), was analyzed. The capillary was inserted into one of the channels in the radial center of the catalyst for gas sampling. By moving this capillary axially within the catalyst channel, gas at various positions along the monolith core was sampled and analyzed. In order to prevent the capillary from dropping out of the channel, only the front 3.6 cm of catalyst was analyzed (catalyst length: 3.8 cm). In order to improve the transient response of the FTIR, N_2 was used to dilute the sample gas and sweep it into the FTIR cell. More detailed information can be found elsewhere [24].

In situ DRIFTS was performed using a Nicolet Nexus 470 spectrometer, equipped with a smart collector with a dual sample environmental chamber (Thermo Fisher Scientific). The powder sample, with little to no cordierite removed, was mechanically removed from the inside of monolith channels. The feed gas, at a total flow rate of 100 cm^3/min at STP, was mixed using Bronkhorst mass flow controllers; and its composition, with all gases present, was 600 ppm NH_3, 600 ppm NO_x, 200 ppm C_3H_6, 8% O_2, balanced by He. Before each experiment, the sample was cleaned by heating to 500 °C in an oxidizing environment (8% O_2 in He) for 30 min. Then the sample was cooled to the target temperature and background spectra were obtained.

3. Results and discussion

3.1. Performance check

Initially, a general performance check, with and without C_3H_6, was performed at multiple temperatures. The results of this performance check are shown in Fig. 1. The activity in the absence of C_3H_6 increased with temperature to 250 °C, and then decreased with further temperature increase because of insufficient reductant due to parasitic NH_3 oxidation by O_2. At low temperature 150 °C, the reaction is kinetically limited, and the turnover rate was estimated to be 1.5×10^{-3} s^{-1}, based on the amount of copper present in the sample. With the introduction of 200 ppm C_3H_6, the extent of the performance changes were dependent upon temperature. At 150 °C, C_3H_6 had no effect. At higher temperatures, a negative effect was observed and was most significant at 300 °C. It is worth noting that at 300 °C it was difficult to obtain steady-state performance, because NO_x conversion continued decreasing with extended C_3H_6 exposure, even after 3 h, indicating some poisons were accumulating on the surface. The point used in Fig. 1 was the conversion at 3 h. At higher temperatures, such as 400 or 500 °C, the poisoning effect of C_3H_6 decreased to a large extent. Such a trend, with the

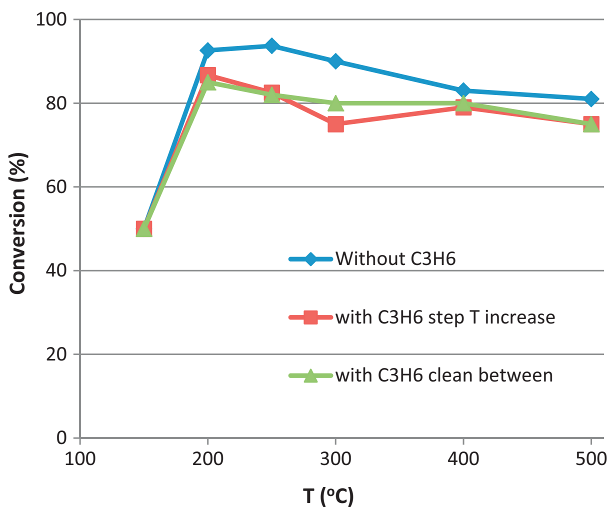

Fig. 1. NO_x conversion under the standard SCR conditions as a function of temperature with/without 200 ppm C_3H_6 (600 ppm NO, 600 ppm NH_3, 8% O_2, 5% CO_2 and 2.5% H_2O, GHSV = 28,000 h^{-1}).

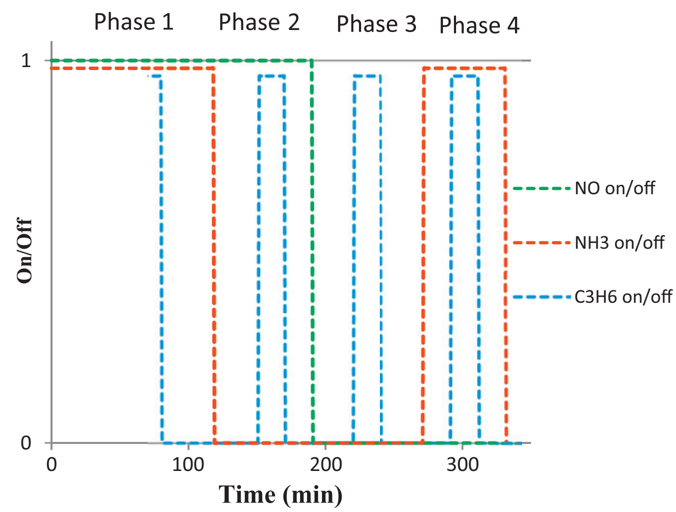

Fig. 2. Four-phase reaction protocol involving the C_3H_6 step-response in each phase.

largest effect by C_3H_6 occurring in the medium temperature range, is consistent with the results over Cu-based zeolite catalysts by Heo et al. and Cavataio et al. [11,14,15].

The performance was checked at each temperature after a step increase, rather than via a temperature ramp, and it could be argued that some degradation occurred at low temperature, such as coke formation or site blocking, that may influence the performance at higher temperature. In order to evaluate this, the performance at each temperature was also measured using a clean surface. Prior to measurement at each temperature, the sample was heated to 550 °C in an oxidizing environment with 600 ppm NO_2 and held for 30 min to remove any possible carbon deposits. These results are also shown in Fig. 1. The measured conversions were similar to those obtained using the sample that was not cleaned between each temperature, indicating it was not carbon deposits formed at low temperature that influenced the performance at higher temperature.

3.2. Step-response method

A step-response method was employed in this study. The advantage of this method is that both the transient and steady state behaviors could be analyzed. Here we used a four-phase reaction protocol as described by Fig. 2. In each phase, a C_3H_6 step was introduced and its effect on different reactions was investigated, including NH_3-SCR (phase 1), HC-SCR or NO oxidation (phase 2), C_3H_6 oxidation (phase 3) and C_3H_6 oxidation in the presence of NH_3, or NH_3 oxidation in the presence of C_3H_6 (phase 4). The focus was phase 1, the SCR reaction, but the other three phases provided details and help explain the SCR reaction results.

The NO, NH_3 and C_3H_6 concentration profiles during the four-phase protocol at 150 °C are shown in Fig. 3. Upon 200 ppm C_3H_6 introduction in phase 1, both the NO and NH_3 concentration showed no change, with C_3H_6 reaching 200 ppm instantly. Meanwhile, there was almost no HC-SCR conversion in phase 2, and no C_3H_6 oxidation in phases 3 and 4. Interestingly, without appreciable NH_3 coverage, some C_3H_6 can be adsorbed, and released slowly once gas-phase C_3H_6 was removed, as shown in phases 2 and 3. However, in the presence of NH_3, upon C_3H_6 introduction or removal, the C_3H_6 concentration increased to 200 ppm or to 0 ppm instantly with no adsorption observed (phases 1 or 4). These results demonstrate that NH_3 strongly inhibits C_3H_6 adsorption. Some C_3H_6 being released at the beginning of phase 4 upon NH_3 introduction lends further evidence. Separate TPD experiments, after adsorption of only C_3H_6, NH_3 or a mixture of the two (results not shown here), show that C_3H_6 adsorption is very weak and the amount adsorbed small, while NH_3 adsorption was substantial (0.005 mmol C_3H_6 vs 0.5 mmol NH_3). C_3H_6 did not compete with NH_3 for adsorption sites.

The four-phase protocol reaction profiles at 250 °C are shown in Fig. 4(a) and an enlarged phase 1 portion in Fig. 4(b). With C_3H_6 introduction, as shown in phase 1, the NO concentration increased from 38 ppm to around 110 ppm. With extended exposure, the NO concentration decreased slowly and reached 100 ppm, higher than that without C_3H_6, indicating the negative effect of C_3H_6. HC-SCR conversion was relatively small (phase 2), and in comparing the C_3H_6 concentrations in phases 3 and 4, it is apparent that the presence of NH_3 significantly decreased C_3H_6 oxidation. The reason for the decreased C_3H_6 oxidation by NH_3 could be due to the inhibition of C_3H_6 adsorption by NH_3, as discussed above. This is reinforced by the observation that for a surface partially covered by NH_3, as would be the case in phase 1 during SCR reaction conditions, the C_3H_6 concentration was between those without NH_3 coverage (phases 2 and 3) and with saturated NH_3 coverage (phase 4).

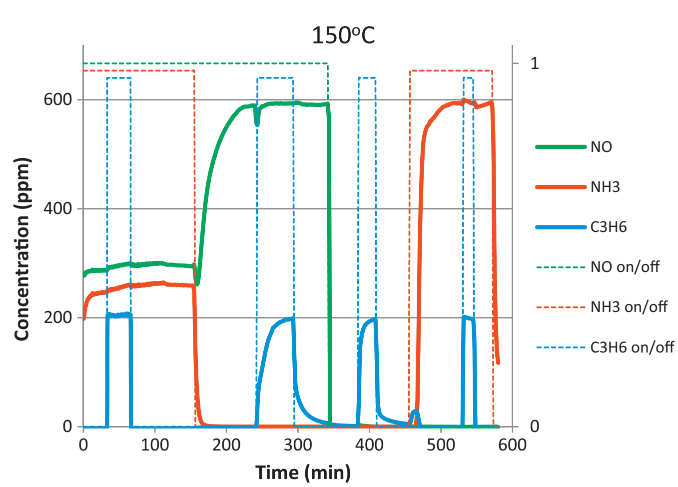

Fig. 3. Outlet gas concentrations during the four-phase reaction protocol at 150 °C; (600 ppm NO, 600 ppm NH_3, 200 ppm C_3H_6, 8% O_2, 5% CO_2 and 2.5% H_2O if required, GHSV = 28,000 h^{-1}).

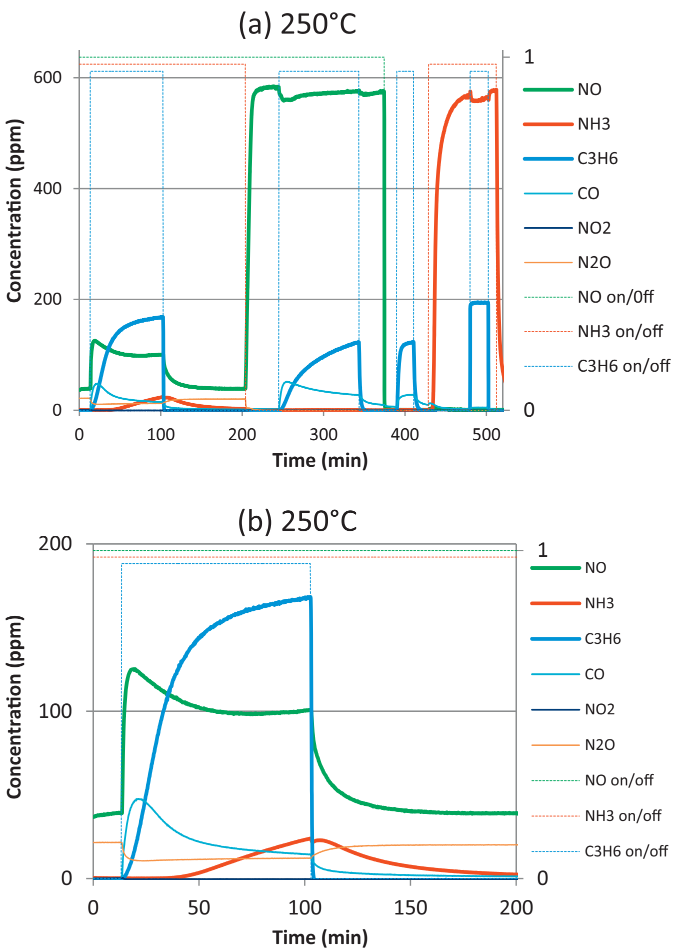

Fig. 4. Outlet gas concentrations during the four-phase reaction protocol at 250 °C (a) and enlarged phase 1 reaction during the C_3H_6 step-response under the standard SCR conditions at 250 °C (b); (600 ppm NO, 600 ppm NH_3, 200 ppm C_3H_6, 8% O_2, 5% CO_2 and 2.5% H_2O if required, GHSV = 28,000 h^{-1}).

Fig. 4(b) highlights the SCR reaction phase of the sequence at 250 °C. As shown, once C_3H_6 was introduced, the NO concentration quickly increased and then decreased slowly before finally reaching a steady value. After extended C_3H_6 exposure (~45 min), NH_3 slip was observed. The coexistence of both NO and NH_3 suggests an insufficient number of active sites for the SCR reaction, and some of the sites, which were active before C_3H_6 introduction, must have been poisoned. Note, the NO concentration jump at the onset of the C_3H_6 addition is not related to temperature change, as this was monitored and found negligible. Also, this sudden increase is not due to the C_3H_6-induced desorption of the adsorbed NO_x, and this can be confirmed by phase 2 of the reaction sequence, since introduction of C_3H_6 to a NO/O_2 pretreated surface did not cause any sudden NO_x release. So the NO concentration increase was related to C_3H_6-induced active site poisoning of the SCR reaction. After C_3H_6 removal, the NO concentration decreased slowly and returned to its original value before C_3H_6 introduction.

As indicated above, some active sites were poisoned by C_3H_6. CO was formed after C_3H_6 introduction, which was due to partial oxidation of C_3H_6, and the NO concentration profiles trends match those of the CO. To determine if CO poisoned the Cu/beta catalyst, as occurs with Pt-based catalysts at low temperature, a separate experiment was performed using a CO step (200 ppm) under SCR conditions at 250 °C. The results (not shown for brevity) indicate that CO had no effect on the SCR reaction at all. Also, the transient increase in NO concentration upon C_3H_6 introduction excludes

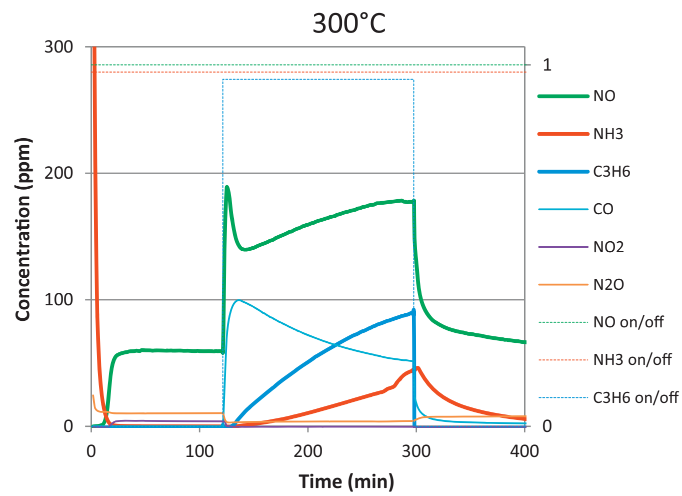

Fig. 5. Outlet gas concentrations during the 200 ppm C_3H_6 step-response under the standard SCR at 300 °C; (600 ppm NO, 600 ppm NH_3, 8% O_2, 5% CO_2 and 2.5% H_2O, GHSV = 28,000 h^{-1}).

poisoning by coke formation, since coke formation is relatively slow and its effect would take some time to build-up. It is more likely that C_3H_6 oxidation intermediates poisoned the catalyst.

The concentration profiles during the SCR phase of the reaction protocol (phase 1) at 300 °C are shown in Fig. 5. The trends were quite similar to those at 250 °C; there was the sudden NO concentration increase once C_3H_6 was introduced and the slower decrease with prolonged exposure, as well as NH_3 breakthrough and the coincident decreased C_3H_6 oxidation. The only difference was that after extended C_3H_6 exposure, the NO concentration began increasing again. The slowly decreasing performance after long-term C_3H_6 exposure was related to coke formation on the surface, with preliminary evidence including the catalyst sample color changing from blue to black after reaction, indicating the formation of coke. DRIFTS results, discussed below, provide further evidence.

The concentration profiles during the SCR phase at 400 °C are shown in Fig. 6. Again, upon C_3H_6 introduction, the NO concentration increased rapidly from 95 ppm to more than 200 ppm. After reaching the maximum, it decreased to a steady-state

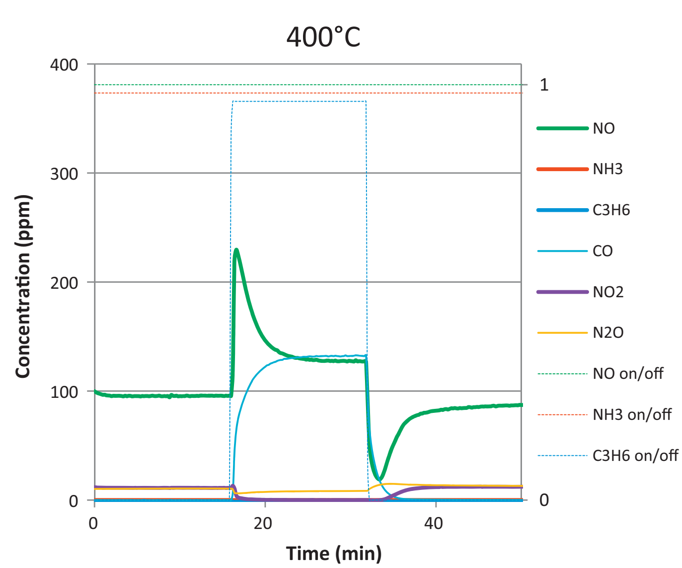

Fig. 6. Outlet gas concentrations during the 200 ppm C_3H_6 step-response under the standard SCR conditions at 400 °C; (600 ppm NO, 600 ppm NH_3, 8% O_2, 5% CO_2 and 2.5% H_2O, GHSV = 28,000 h^{-1}).

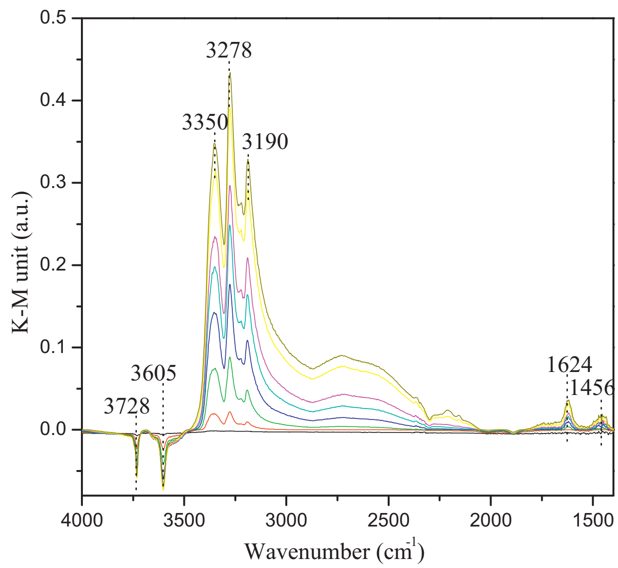

Fig. 7. DRIFTS spectra obtained at different times (0, 2, 4, 6, 8, 10, 20, 30 min) upon Cu/beta exposure to 600 ppm NH_3 at 250 °C; (600 ppm NH_3, 8% O_2, balanced by He).

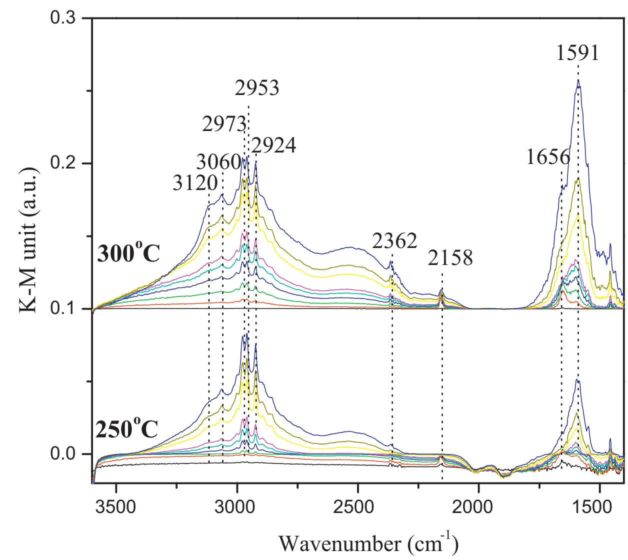

Fig. 8. DRIFTS spectra obtained at different times (0, 2, 4, 6, 8, 10, 20, 30, 60 min) upon Cu/beta exposure to 200 ppm C_3H_6 at 250 °C (bottom) and 300 °C (top); (200 ppm C_3H_6, 8% O_2, balanced by He).

concentration of 127 ppm. NO_2 was evident before C_3H_6 was added, but was not observed after C_3H_6 was added. Also, no NH_3 slip was observed after C_3H_6 was added. After C_3H_6 was removed from the gas feed, the outlet NO concentration decreased to a value lower than that prior to C_3H_6 addition, and then returned to its original concentration, and NO_2 was again evident. Data were also obtained at 500 °C (again, not shown for brevity) with the trends similar to those observed at 400 °C, albeit with less inhibition noted.

In summary, the negative effect of C_3H_6 on the SCR reaction was confirmed by these step-response experiments, especially at 250 and 300 °C. The deactivation was not related to competitive adsorption between NH_3 and C_3H_6, or CO poisoning, but was related to poisoning of some active sites, possibly by C_3H_6 oxidation intermediates. At least two types of intermediates exist, one contributed to the sudden NO concentration increase once C_3H_6 was introduced, and the other is associated with coke, which was responsible for the slow NO concentration increase with time. In order to identify these poisons, in situ DRIFTS was used.

3.3. *In situ DRIFTS*

First, NH_3 adsorption was investigated in the presence of O_2 at 250 °C, and the spectra, as a function of adsorption time, are shown in Fig. 7. Bands associated with NH_3 adsorption developed at 3190, 3278 and 3350 cm^{-1}, and can be assigned to N–H vibrations [25]. Small bands at 1624 cm^{-1} and 1456 cm^{-1}, which are attributed to Lewis acid-bound NH_3 and protonated NH_3, respectively, also appeared [26]. As a result of NH_3 adsorption and interaction with the surface, negative bands at 3605 cm^{-1} and 3728 cm^{-1}, which can be assigned to Si—OH—Al and Si—OH, respectively, were observed [27]. Similar bands were identified in the tests performed at 300 °C, only with lower intensity. When NH_3 and NO were added together, the same spectra as those with only NH_3 present were obtained, indicating adsorbed NH_3 species dominated the surface during the SCR reaction.

The spectra obtained when the sample was exposed to C_3H_6 under oxidizing conditions, at both 250 and 300 °C are shown in Fig. 8. Once C_3H_6 was introduced, a band at 1656 cm^{-1} first appeared, which can be attributed to a C═O bond vibration of acrolein (CH_2═CH—CHO) [28,29], considering some C—H bond vibrations around 2950 cm^{-1} were observed. Upon extended C_3H_6 exposure, bands at 1591 cm^{-1} and above 3000 cm^{-1}, such as at 3020 and 3120 cm^{-1}, appeared and grew with time. According to Krishna and Makkee [30], who investigated the interaction of C_3H_6 with HZSM5 in an oxidizing environment, bands above 3000 cm^{-1} and at 1600–1550 cm^{-1} correspond to the C—C and C—H stretching vibrations, respectively, of condensed aromatic rings (hydrogen deficient), or in other words coke. Therefore, coke was formed on the catalyst surface. The formation of coke was also qualitatively confirmed by the sample color change from blue to slightly black at the end of these experiments. In addition, small bands at 2158 and 2362 cm^{-1} were evident, and were attributed to CO adsorbed on Cu^+ and gas phase CO_2, respectively [31].

In a separate series of experiments, after the catalyst surface was exposed to a gas mixture of NO, NH_3 and O_2, C_3H_6 was then introduced and spectra were obtained as a function of exposure time, with data shown in Fig. 9. Data obtained at 250 °C are shown in Fig. 9(a). Prior to C_3H_6 introduction, the catalyst surface was predominantly covered by NH_3, as indicated by the strong N—H bands above 3000 cm^{-1}, and these bands decreased in intensity with time after C_3H_6 introduction, because of NH_3 desorption and oxidation by O_2. A strong band at 2162 cm^{-1}, assigned to CO adsorbed on Cu^+, developed, along with a small shoulder at 2218 cm^{-1} due to NCO^- adsorbed over Cu^+ [25,31]. Also, bands at 2968 cm^{-1} and 1662 cm^{-1}, corresponding to acrolein (CH_2═CH—CHO) species, were observed. Since CO had no effect on the SCR reaction at 250 °C as shown in the results above, it is inferred from these DRIFTS results that these acrolein species poisoned the SCR activity, possibly by strongly adsorbing over the active copper sites and preventing SCR functionality.

The spectra obtained during exposure of the catalyst to C_3H_6 after NO + NH_3 + O_2 at 300 °C are shown in Fig. 9 (b). As at 250 °C, prior to C_3H_6 introduction, the catalyst surface was covered by NH_3, but to a lesser degree as indicated by the lower intensity. After C_3H_6 introduction, again similar to the results at 250 °C, bands due to acrolein species formation, at 2968 and 1662 cm^{-1}, developed. However, new bands appeared at 3060 and 1592 cm^{-1} as well, indicating that coke was formed on the catalyst surface at 300 °C. Adsorbed CO and NCO^- were also identified; however, NCO^- was positioned on zeolite sites instead of Cu^+, since the band was shifted from 2218 cm^{-1} to 2250 cm^{-1} [27,31], possibly due to its migration from Cu^+ to the zeolite support.

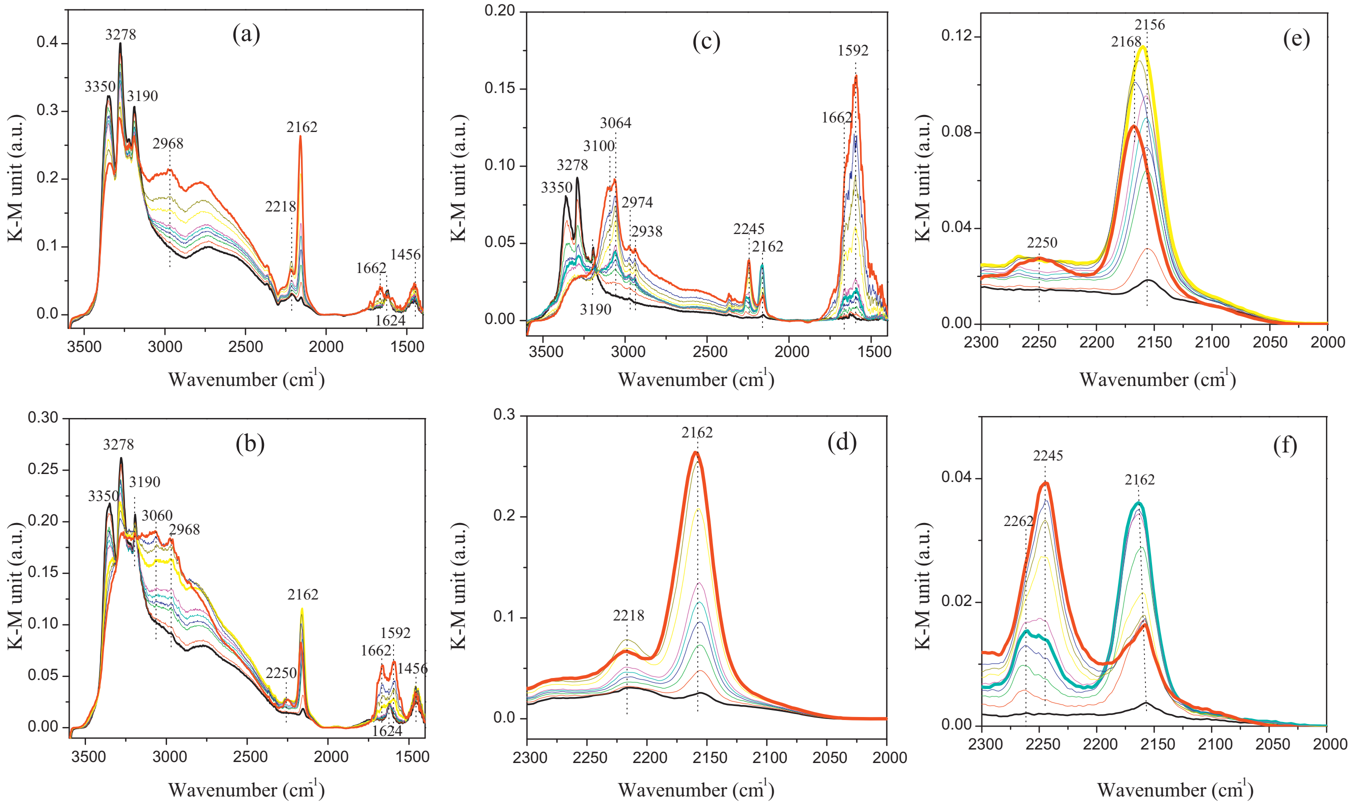

Fig. 9. DRIFTS spectra obtained at different times (0, 2, 4, 6, 8, 10, 20, 30, (40), 60 min) upon Cu/beta exposure to 200 ppm C_3H_6 after NH_3 pre-saturation at 250 °C (a), 300 °C (b), 400 °C (c) and the corresponding enlarged region of CO adsorption on Cu^+ at 250 °C (d), 300 °C (e) and 400 °C (f); (200 ppm C_3H_6, 8% O_2, balanced by He).

Spectra obtained during C_3H_6 exposure at 400 °C after exposure to NO + NH_3 + O_2 are plotted in Fig. 9(c). Coke, or more specifically, more hydrogen-deficient aromatics, possibly including some polyaromatics, accumulated on the surface, as indicated by the strong bands above 3000 cm^{-1} (3100 and 3064 cm^{-1}) and 1592 cm^{-1} [30,32]. The bands at around 2950 cm^{-1} and 1662 cm^{-1}, due to the oxidation intermediates, were relatively weaker. In addition, bands associated with CO adsorbed on Cu^+ and NCO^- adsorbed on zeolite were also present.

Fig. 9(d)–(f) highlight the CO adsorption band over Cu^+, at 2162 cm^{-1}, at multiple temperatures. With the understanding that CO does not affect SCR performance, this band intensity can be used to evaluate the accessibility of the active copper sites. At 250 °C, this band increased in intensity first and then reached a steady-state maximum. At 300 °C, it initially increased, but after 20 min began, and continued, to decrease. Similar phenomena were also observed at 400 °C, except that the band reached a steady-state intensity. Thus, under SCR conditions with C_3H_6 present, coke was formed at 300 and 400 °C but not at 250 °C. Coincident with the changes in the adsorbed CO data, this demonstrates that the availability of Cu^+ sites decreased, possibly by being covered by the carbon deposits or these blocking the zeolite pores.

In evaluating the results from DRIFTS and step-response experiments, the types of poisons and their effects can be characterized. Acrolein species develop from C_3H_6 partial oxidation and poison the catalyst, leading to the sudden NO concentration increase at the onset of C_3H_6 introduction, while the coke formed at 300 °C was responsible for the slow increase in NO concentration with extended C_3H_6 exposure, since it decreased the number of active copper sites as it accumulated on the surface. Although coke was also formed at 400 °C and resulted in blocking some copper sites, there were enough remaining active sites for significant SCR reaction due to the higher temperature and thus turnover frequency and possibly coke oxidation. Enough active sites are confirmed by the absence of NH_3 breakthrough with extended C_3H_6 exposure.

With respect to coke formation, at 250 °C, coke formed on a clean surface as indicated by Fig. 8, while coke was not observed on a NH_3 pre-adsorbed surface as shown by Fig. 9(a). Also, the coke band at 300 °C was more intense for the clean surface than that on the NH_3-covered surface. This indicates that NH_3 adsorption, to some extent, inhibited coke formation. Also, as discussed above, NH_3 inhibited C_3H_6 adsorption and subsequent oxidation, demonstrated by the decreased C_3H_6 conversion in the presence of NH_3 shown in Fig. 10 when comparing the results from phases 3 and 4 of the protocol at different temperatures. Therefore, as would be expected, coke formation, and the amount formed, is possibly related to the extent of

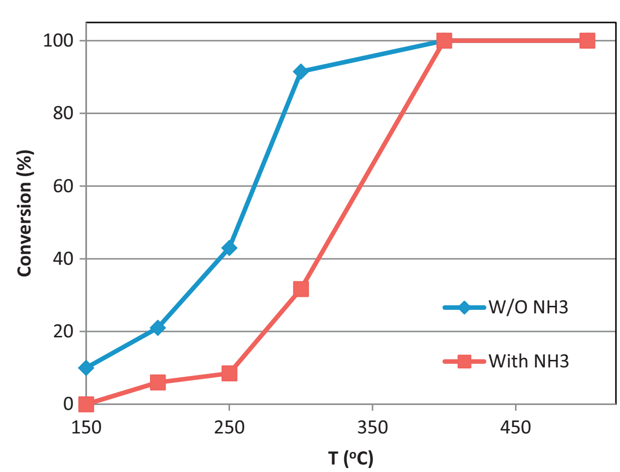

Fig. 10. C_3H_6 oxidation conversion with or without 600 ppm NH_3 (200 ppm C_3H_6, 8% O_2, 5% CO_2 and 2.5% H_2O, GHSV = 28,000 h^{-1}).

C_3H_6 oxidation. Further verification was obtained by exposing the sample to C_3H_6 at 300 °C, after NH_3 adsorption, but in the absence of O_2, and little coke was formed (results not shown). With this basis, it is very possible that coke formed through the condensation and rearrangement of oxidation intermediates, such as the observed acrolein species, with the possible reason being their enhanced deposition ability on the surface, as compared to C_3H_6. Previous results, reporting enhanced coke deposition during C_3H_6-SCR over ZSM-5 [30], are consistent with these findings.

In summary, C_3H_6 oxidation intermediates, not C_3H_6 itself, poisoned the catalyst. At low temperature, 150 °C, there was no C_3H_6 oxidation, and therefore no effect of C_3H_6 on the SCR reaction was observed. At 250 °C, oxidation intermediates poisoned the catalyst, leading to the rapid NO concentration increase once C_3H_6 was introduced. At 300 °C, in addition to acrolein-like species, coke accumulated on the surface and blocked some of the active sites, leading to the subsequent slow performance decrease. At high temperature, 400 °C, the performance was not limited by an insufficient number of active sites. Although coke was also formed, some sites remained active. Instead, as there was no NH_3 slipping through the catalyst, NO_x conversion was ultimately limited by insufficient NH_3 supply, via NH_3 oxidation. The results also indicated that NH_3 consumption was slightly promoted in the presence of C_3H_6 (not shown). Therefore, NO_x conversion decreased slightly at high temperature due to less available NH_3 for the SCR reaction. The promoted NH_3 consumption in the presence of C_3H_6 was also observed by Heo et al. and was attributed to NH_3 oxidation and ammoxidation reactions [15]. The DRIFTS results shown in Fig. 9 suggest that NCO^- species were formed after C_3H_6 exposure to a NH_3-adsorbed surface, suggesting some interaction between C_3H_6 and NH_3, which possibly promoted NH_3 consumption.

3.4. NO concentration change behavior

The first increase in NO_x once C_3H_6 was introduced was due to catalyst poisoning by C_3H_6 partial oxidation products, and the slowly increasing NO_x concentration with extended C_3H_6 exposure at 300 °C was due to coke formation. However, there was a NO concentration reduction between these stages, soon after the NO increase at the onset of C_3H_6 addition. This phenomenon is believed to be related to NH_3 adsorption along the catalyst. To demonstrate this hypothesis, spaci-FTIR was used to spatially resolve the reactions along the monolith sample. Fig. 11 shows steady-state NO and NH_3 concentrations as a function of catalyst length at multiple temperatures. At 150 °C, NO and NH_3 concentrations decreased monotonically along the catalyst. At 200 °C, not all the catalyst was used, and the front 2 cm catalyzed all the NO reduction, therefore implying that all adsorbed NH_3 was located in this region. As temperature increased, the reaction zone moved farther to the front (within 1 cm at 300 °C and 0.7 cm at 400 °C) and NO reduction became limited by NH_3 supply, since more NH_3 was also oxidized by O_2.

The spaci-FTIR data indicated that at 200 °C or higher, only the catalyst front was used for reaction, and therefore this was where adsorbed NH_3 resided. In combining these results with the C_3H_6 poisoning trends, the NO and NH_3 concentration profiles can be described. For example at 250 °C, initially, in the absence of C_3H_6, the steady-state SCR reaction occurred in the front only, with NO and NH_3 concentrations decreasing rapidly. Once C_3H_6 was added, some active sites in this small reaction zone at the front were partially, and quickly, poisoned by C_3H_6 oxidation intermediates. This caused the NO concentration in the effluent to increase to the higher value. However, as a result of the decreased NO conversion, less NH_3 was consumed. With extended exposure time, this "extra" NH_3 was then adsorbed on the catalyst at sites downstream of the initial reaction zone, and adsorbed NH_3 therefore penetrated farther along

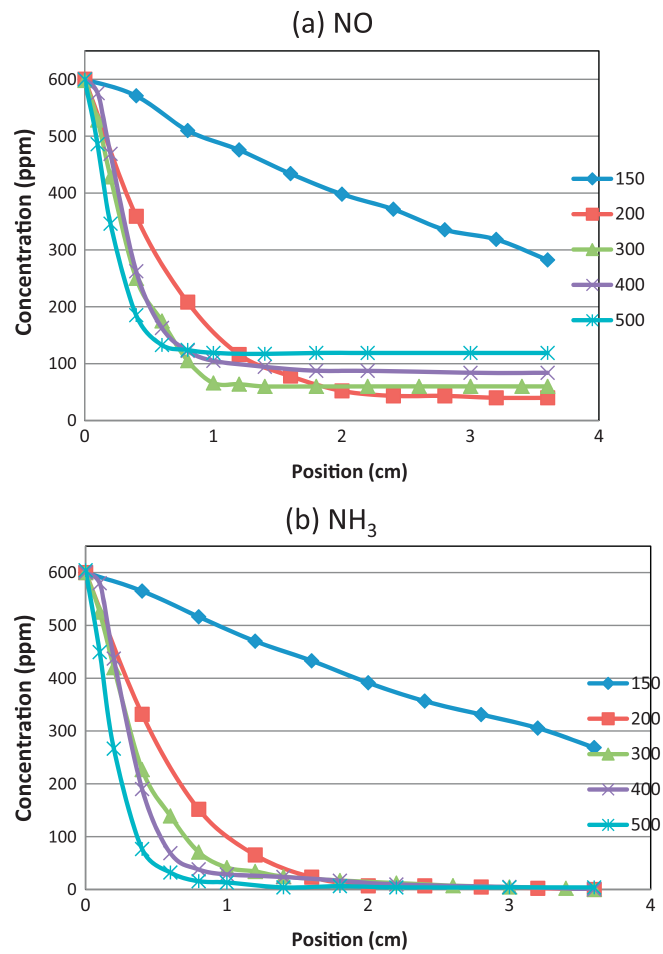

Fig. 11. Spatially resolved steady-state NO (a) and NH_3 (b) concentrations at different temperatures under the standard SCR conditions (600 ppm NO, 600 ppm NH_3, 8% O_2, 5% CO_2 and 2.5% H_2O, GHSV = 28,000 h^{-1}).

the catalyst. As NH_3 adsorbed downstream along the catalyst, the reaction zone expanded, occurring wherever reductant NH_3 was present. Some of the active sites that were not initially utilized before were then used for NO_x reduction, leading to the subsequent decrease in NO concentration. This indicates that although the catalyst was poisoned by C_3H_6 oxidation intermediates, not all the active sites were poisoned, and some of them remained active for SCR. Lastly, just before NH_3 break-through was observed, all the downstream sites were being used, and the NO concentration decrease stopped, as shown in Fig. 4(b), where NO reached a steady concentration just when NH_3 was measured at the outlet.

At 300 °C, due to the accumulation of coke, the NO concentration increased again after this decrease with the expanding reaction front. The effect of coke accumulation was slow and thus took a longer time period to evolve. At 400 °C, the reaction zone again expanded, but this zone did not extend through the entire catalyst since there was no NH_3 breakthrough. Some of the active sites remained active in this longer reaction zone, and were numerous enough to consume NH_3. The presence of the extended reaction zone is verified by the NO concentration change once C_3H_6 was removed. As shown in Fig. 6, the NO concentration decreased for some time after C_3H_6 removal, to a value even lower than that before C_3H_6 introduction. This was because of the increased NH_3 coverage, as well as quick regeneration of some of the coke-poisoned sites. The data indicate that even with extensive exposure to C_3H_6, some activity persisted. At the higher temperatures, these remaining active sites can be either coke resistant or coke may be

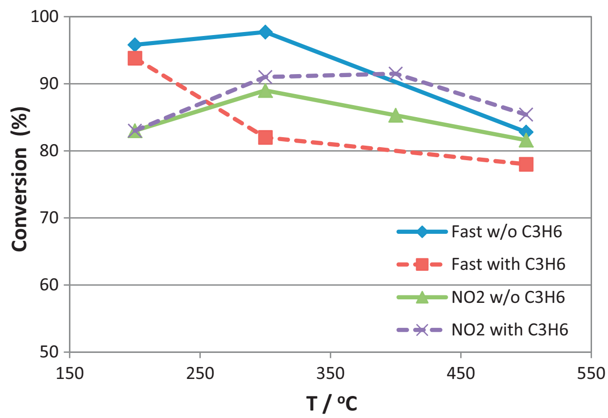

Fig. 12. NO_x conversion under fast and NO_2 SCR conditions as a function of temperature with/without 200 ppm C_3H_6 (600 ppm NO_x, 600 ppm NH_3, 8% O_2, 5% CO_2 and 2.5% H_2O, GHSV = 28,000 h^{-1}).

quickly oxidized and removed if formed. At 300 °C, the reaction was not run long enough to determine if active sites would remain with coke saturation.

3.5. Effect of C_3H_6 on the fast SCR and NO_2 SCR

The effects of C_3H_6 on the fast SCR and NO_2 SCR reactions were also investigated. NO_x conversions at different temperatures, with or without C_3H_6, are shown in Fig. 12. For the fast SCR reaction, C_3H_6 had a similar negative effect as was observed with the standard SCR, especially in the medium temperature range, 300 °C. For NO_2 SCR, C_3H_6 had a slightly positive effect.

Phase 1 of the reaction protocol, which was used to evaluate the effect of C_3H_6 on SCR, at 300 °C is shown in Fig. 13 for the fast SCR reaction conditions. Although the fast SCR reaction occurs via a different reaction pathway, all the gas concentration profiles changed similarly to those under standard SCR reaction conditions, such as NH_3 breakthrough, and the rapid NO concentration increase, slow decrease and then subsequent increase.

The effect of C_3H_6 on the NO_2 SCR reaction at 300 °C is shown in Fig. 14. Before C_3H_6 introduction, 67 ppm NO_2 was unconverted. With C_3H_6 introduction, NO_2 disappeared and around 80 ppm NO was observed during the transient. The slightly increased NO_x concentration is probably related to copper site poisoning, but the poisoning is much weaker compared to the standard and fast SCR reaction conditions, due to the co-existence of some beneficial

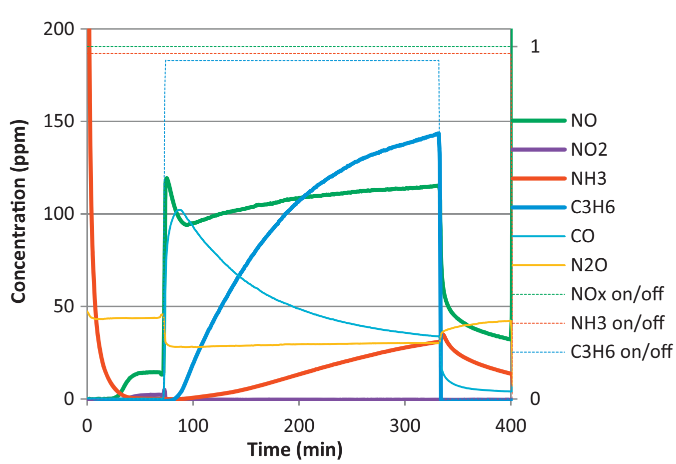

Fig. 13. Outlet gas concentrations during the 200 ppm C_3H_6 step-response under the fast SCR conditions at 300 °C; (300 ppm NO, 300 ppm NO_2, 0 or 200 ppm C_3H_6, 600 ppm NH_3, 8% O_2, 5% CO_2 and 2.5% H_2O, GHSV = 28,000 h^{-1}).

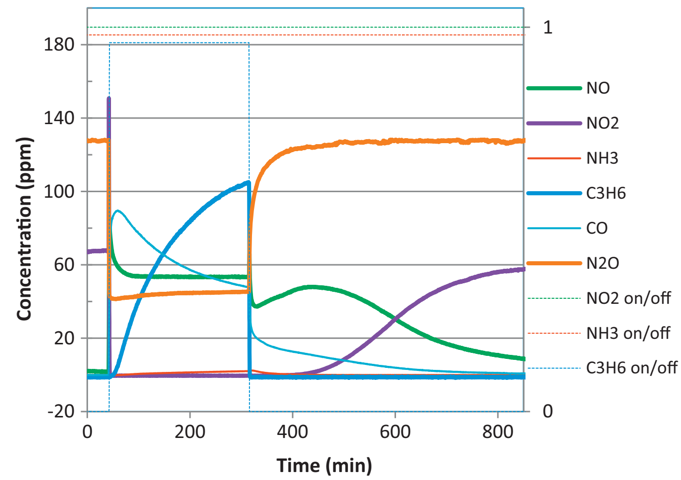

Fig. 14. Outlet gas concentrations during the 200 ppm C_3H_6 step-response under NO_2 SCR conditions at 300 °C; (600 ppm NO_2, 600 ppm NH_3, 0 or 200 ppm C_3H_6, 8% O_2, 5% CO_2 and 2.5% H_2O, GHSV = 28,000 h^{-1}).

effects of C_3H_6 on NO_2 reduction, including HC-SCR (NO_2 + HC) and reaction route change (discussed below) which will contribute to NO_x reduction. With extended exposure, the NO concentration gradually decreased to 53 ppm. Again, the decrease is related to NH_3 adsorbed along a longer length of catalyst, due to fact that C_3H_6 can serve as a relatively efficient reductant for NO_2 (25% conversion by 600 ppm NO_2 and 200 ppm C_3H_6) which can free some NH_3. A larger extent of NH_3 adsorption is also confirmed by the decreased NO_x concentration (from 53 to 38 ppm) once C_3H_6 was turned off. Overall, the presence of C_3H_6 leads to slightly improved steady-state NO_x conversion. Meanwhile, N_2O formation decreased substantially with C_3H_6 addition, from 127 ppm to 44 ppm. During NO_2 SCR, significant quantities of N_2O can be formed due to the decomposition of ammonium nitrates [33,34], which results from reaction between NO_2 and NH_3. Therefore, C_3H_6 must ultimately decrease the formation of ammonium nitrates, with the intrinsic reason being the reduction of NO_2 by C_3H_6 to NO. During phase 2 of the reaction protocol, which was used to characterize HC-SCR, 600 ppm NO_2 and 200 ppm C_3H_6 were introduced, and 450 ppm NO and 0 NO_2 was measured (data not shown here), indicating the reduction of NO_2 by C_3H_6 to NO and N_2.

With these data, it was apparent that some portion of the NO_2 is reduced to NO if C_3H_6 is present. The consequences are that under the fast SCR reaction conditions, the addition of C_3H_6 may cause some of the NO_2 to be reduced to NO and therefore it is not only fast SCR conditions that exist, but both the standard and the fast SCR reaction occurring simultaneously. For NO_2 SCR, some of the NO_2 was reduced to NO, resulting in some portion of fast SCR conditions since both NO and NO_2 are then present. Therefore, the fast SCR reaction was affected by C_3H_6 in the same way as the standard SCR reaction, with the complex NO concentration profile change, while under NO_2 SCR conditions in the presence of C_3H_6, the fast SCR reaction and NO_2 SCR occurred simultaneously, instead of pure NO_2 SCR, also confirmed by the significantly decreased N_2O formation. In addition, under NO_2-SCR reaction conditions, coke was formed on the catalyst surface in the presence of C_3H_6. This can be deduced from the CO formed after C_3H_6 was removed, and long-term NO formation before NO_2 finally appeared, which was due to the oxidation of residual coke on the surface, by NO_2 with the formation of NO. Although coke was formed under NO_2 SCR conditions, NO conversion did not decrease, which differs from the trends observed under both standard and fast SCR conditions. This suggests that enough active sites were still available for the reaction. As indicated here, fast or NO_2 SCR actually occurred instead of

standard SCR, and the TOF of the active sites toward these reactions, especially fast SCR, might be much higher compared to standard SCR, so it is very possible that high conversions were achieved within the upstream portion of the catalyst, where it would be difficult to form coke since it could be removed quickly by NO_2, known to be a strong oxidant. Thus the coke would be formed downstream, where all the NO_2 would be consumed, or where conversion was complete.

Finally, in order to confirm the reduction of NO_2 to NO by C_3H_6, spaci-FTIR was applied to probe the reaction patterns inside the monolith channel. First, the fast SCR reaction with or without C_3H_6 added was investigated, and the spatially resolved gas-phase NO and NO_2 concentrations soon after C_3H_6 introduction (within 30 min) are shown in Fig. 15(a). For the fast SCR reaction without C_3H_6 (measured before C_3H_6 introduction), the consumption of NO_2 and NO were very close, with slightly more NO_2 consumption; however, in the presence of C_3H_6, NO_2 consumption as a function of catalyst length, or residence time, did not change, while NO consumption was much smaller.

The spatially resolved NO, NO_2 and N_2O concentrations under inlet NO_2 SCR conditions, with and without C_3H_6 are shown in Fig. 15(b). At the catalyst inlet, there is little to no change in NO_2 consumption observed, with some NO_2 reduced to NO by C_3H_6 observed at about 0.4 cm. The biggest difference with the addition of C_3H_6 was the significantly decreased N_2O formation, further verifying NO_2 was reduced to NO by C_3H_6, leading to the simultaneous occurrence of the fast and NO_2 SCR reactions instead of purely NO_2 SCR.

Finally, the reduction of NO_2 to NO by C_3H_6 was spatially resolved, to determine the relative rate of this reaction, as compared to fast or NO_2 SCR. The results are shown in Fig. 15(c). Clearly, the reduction proceeded at a very fast rate, with the reaction completed in the front 0.9 cm, comparable in rate to the fast SCR and NO_2 SCR reactions. Meanwhile, some HC-SCR activity was observed between NO_2 and C_3H_6, since less than 500 ppm of NO was observed in the effluent with 600 ppm NO_2 added in the feed. Considering the relative rates, the co-occurrence of NO_2 reduction to NO and SCR reaction is possible. Furthermore, these two reactions could be coupled since the reduction product NO would then be a reactant for the fast SCR reaction.

4. Conclusions

C_3H_6 inhibits the SCR reaction over a Cu/beta SCR catalyst. Adsorption measurements show that C_3H_6 did not influence NH_3 adsorption. DRIFTS and reactor data show that C_3H_6 oxidation intermediates, but not C_3H_6 itself, poison the Cu/Beta SCR catalyst. At temperatures below the onset of C_3H_6 oxidation, there was no effect of C_3H_6 on SCR performance. At temperatures in the range of 250 °C, acrolein-like intermediates poisoned the copper sites and at 300 °C coke was formed possibly due to condensation of the intermediates in addition to poisoning by these acrolein-like species. Both the acrolein-like species and the coke led to decreased performance by masking the copper sites. At higher temperatures, 400 °C and above, the negative effects of C_3H_6 decreased since the number of active sites was sufficient for NO_x reduction, due to quick poison removal if formed and enhanced turnover frequency. Instead, NO_x conversion was limited by reductant supply, due to increased NH_3 oxidation by O_2. Since C_3H_6 slightly promoted extra NH_3 consumption, less NH_3 was available for SCR reaction, and a slightly negative effect of C_3H_6 was still observed. The presence of NH_3 was found to inhibit C_3H_6 oxidation, therefore delaying the formation of coke to some extent at 250 °C.

For the fast SCR reaction, C_3H_6 had a similarly negative effect, since some of the NO_2 was reduced to NO by C_3H_6, leading to

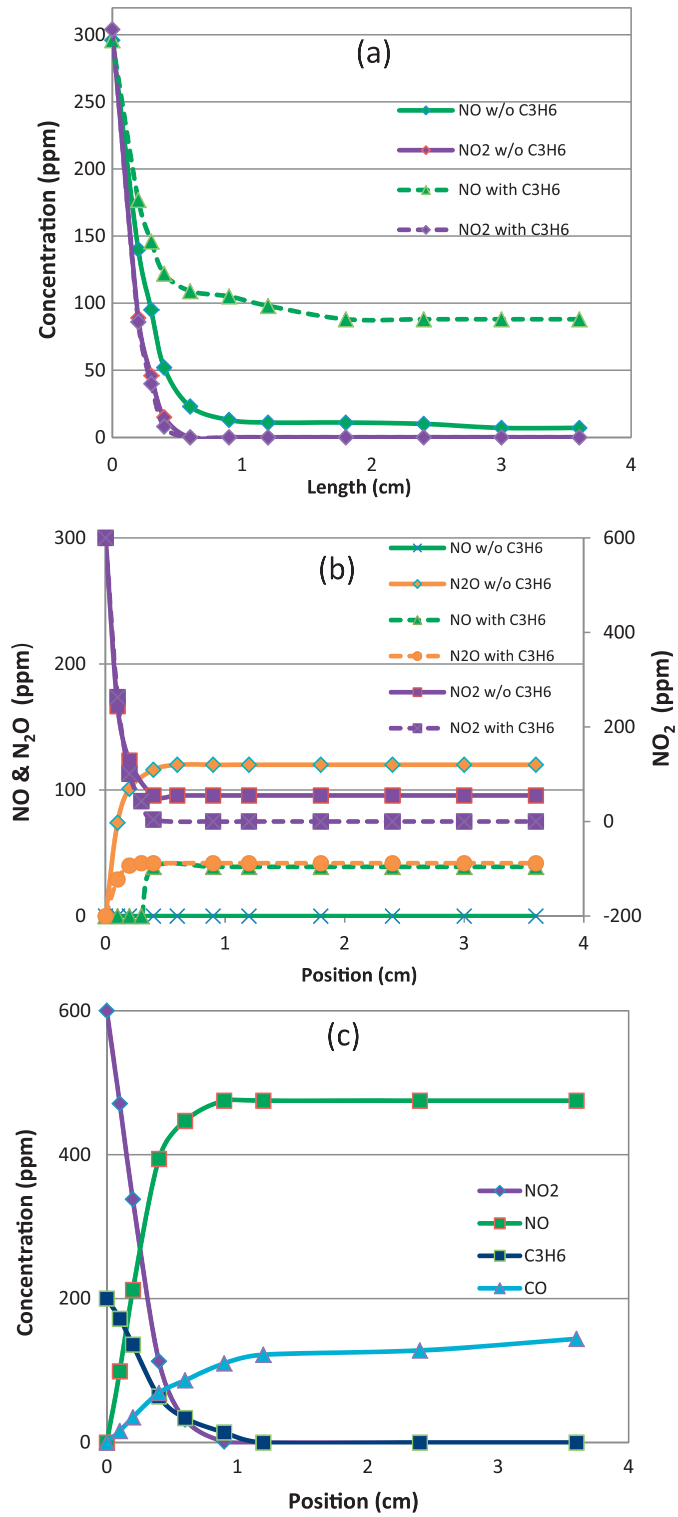

Fig. 15. Spatially resolved NO, NO_2, CO, N_2O and C_3H_6 gas concentrations at 300 °C (a) under the fast SCR conditions with or without C_3H_6; (b) under NO_2 SCR conditions with or without C_3H_6; and (c) with only NO_2 and C_3H_6 introduced (600 ppm NO_x, 600 ppm NH_3, 200 ppm C_3H_6, 8% O_2, 5% CO_2 and 2.5% H_2O, except (c) which contained no NH_3, GHSV = 28,000 h^{-1}).

the co-occurrence of standard SCR instead of purely fast SCR. However, C_3H_6 had a positive effect on NO_2 SCR for the same reasons. The reduction of NO_2 to NO resulted in the co-occurrence of the fast SCR reaction instead of purely NO_2 SCR, also leading to greatly decreased N_2O formation. Both the change in reaction

pathway and HC-SCR (NO_2 and C_3H_6) contributed to enhanced NO_x conversion by C_3H_6 under NO_2 SCR conditions.

Acknowledgement

The authors gratefully acknowledge Cummins Inc for the sample provided and funding for this work.

References

[1] T.V. Johnson, SAE Technical Paper 2011-01-0304.
[2] M. Koebel, M. Elsener, M. Kleemann, Catalysis Today 59 (2000) 335–345.
[3] H.Y. Chen, E.C. Weigert, J.M. Fedeyko, J.P. Cox, P.J. Andersen, SAE Technical Paper 2010-01-0302.
[4] W. Li, K.L. Perry, K. Narayanaswamy, C.H. Kim, P. Najt, SAE Technical Paper 2010-01-0366.
[5] C.L. DiMaggio, G.B., Fisher, K.M., Rahmoeller, M. Sellnau, SAE Technical Paper 2009-01-0277.
[6] K. Kamasamudram, N.W. Currier, T. Szailer, A. Yezerets, SAE Technical Paper 2010-01-1182.
[7] T.J. Toops, K. Nguyen, A.L. Foster, B.G. Bunting, N.A. Ottinger, J.A. Pihl, E.W. Hagaman, J. Jiao, Catalysis Today 151 (2010) 257–265.
[8] D.W. Fickel, E. D'Addio, J.A. Lauterbach, R.F. Lobo, Applied Catalysis B 102 (2011) 441–448.
[9] J.M. Fedeyko, H.Y. Chen, T.H. Ballinger, E.C. Weigert, H.L. Chang, J.P. Cox, P.J. Andersen, SAE Technical Paper 2009-01-0899.
[10] S.J. Schmieg, J.W. Lee, SAE Technical Paper 2005-01-3881.
[11] G. Cavataio, J.R. Warner, J.W. Girard, J. Ura, D. Dobson, C.K. Lambert, SAE Technical Paper 2009-01-0903.
[12] P. Kern, M. Klimczak, T. Heinzelmann, M. Lucas, P. Claus, Applied Catalysis B 95 (2010) 48–56.
[13] P.J. Andersen, H.Y. Chen, J.M. Fedeyko, E. Weigert, US Patent 2010/0267548 A1.
[14] I. Bull, W.M. Xue, P. Burk, R.S. Boorse, W.M. Jaglowski, G.S. Koermer, A. Moini, J.A. Patchett, J.C. Dettling, M.T. Caudle, US Patent US 7,601,662 B2.
[15] I. Heo, Y. Lee, I.S. Nam, J.W. Choung, J.H. Lee, H.J. Kim, Microporous and Mesoporous Materials 14 (2011) 8–15.
[16] J.H. Li, R.H. Zhu, Y.S. Cheng, C.K. Lambert, R.T. Yang, Environmental Science and Technology 44 (2010) 1799–1805.
[17] C. He, Y. Wang, Y. Cheng, C.K. Lambert, R.T. Yang, Applied Catalysis A 368 (2009) 121–126.
[18] I. Malpartida, O. Marie, P. Bazin, M. Daturi, X. Jeandel, Applied Catalysis B 102 (2011) 190–200.
[19] M. Devarakonda, R. Tonkyn, D. Herling, SAE Technical Paper 2010-01-1171.
[20] C. Montreuil, C. Lambert, SAE Technical Paper 2008-01-1030.
[21] A. Sultana, T. Nanba, M. Sasaki, M. Haneda, K. Suzuki, H. Hamada, Catalysis Today 164 (2011) 495–499.
[22] T. Nanba, A. Sultana, S. Masukawa, M. Haneda, J. Uchisawa, A. Obuchi, H. Hamada, Topics in Catalysis 52 (2009) 1766–1770.
[23] J. Girard, R. Snow, G. Cavataio, C. Lambert, SAE Technical Paper 2008-01-0767.
[24] J.Y. Luo, X. Hou, P. Wijayakoon, S.J. Schmieg, W. Li, W.S. Epling, Applied Catalysis B 102 (2011) 110–119.
[25] F. Poignant, J. Saussey, J.C. Lavalley, G. Mabilon, Catalysis Today 29 (1996) 93–97.
[26] D. Klukowski, P. Balle, B. Wagloehner, S. Kureti, B. Kimmerle, A. Baiker, J.D. Grunwaldt, Applied Catalysis B 93 (2009) 185–193.
[27] L. Capek, K. Novoveska, Z. Sobalik, B. Wichterlova, L. Cider, E. Jobson, Applied Catalysis B 60 (2005) 201–210.
[28] R.Q. Long, R.T. Yang, Journal of Physical Chemistry B 103 (1999) 2232–2238.
[29] N. Sivasankar, H. Frei, Journal of Physical Chemistry C 115 (2011) 7545–7553.
[30] K. Krishna, M. Makkee, Applied Catalysis B 59 (2005) 35–44.
[31] J.A. Anderson, C.M. Alwarez, M.J.L. Munoz, I.R. Ramos, A.G. Ruiz, Applied Catalysis B 14 (1997) 189–202.
[32] M. Guisnet, P. Magnoux, Applied Catalysis A 212 (2001) 83–96.
[33] A. Grossale, I. Nova, E. Tronconi, D. Chatterjee, M. Weibel, Journal of Catalysis 256 (2008) 312–322.
[34] A. Grossale, I. Nova, E. Tronconi, Journal of Catalysis 265 (2009) 141–147.